Reviews on Advanced Materials and Technologies, 2024, vol. 6, no. 3, pp. 120–131
DOI: 10.17586/2687-0568-2024-6-3-120-131

Hydrogen-Enhanced Martensitic Transformation and Twinning under Rolling of AISI 321 Austenitic Stainless Steel

Elena G. Astafurova*, Evgenii V. Melnikov, Sergey V. Astafurov

Laboratory of Physics of Hierarchical Structures in Metals and Alloys, Institute of Strength Physics and Materials Science SB RAS, 2/4 Akademicheskii prospekt, 634055, Tomsk, Russia

Article history

Received September 20, 2024
Accepted September 25, 2024
Available online September 30, 2024

Abstract

In this paper, we study the effect of hydrogen pre-charging (in a 1N H_2SO_4 solution with a $CS(NH_2)_2$ as a recombination potion, at current densities of 10, 100 and 200 mA/cm^2, for 5 hours) on the microstructure and phase composition of a type AISI 321 austenitic stainless steel during room-temperature rolling. Hydrogen pre-charging enhances the contribution of mechanical twinning to the fragmentation of the structure and assists to γ→α' and γ→ε transformations during rolling. Both, twinning and martensitic transformations, are dependent on hydrogen pre-charging regime: an increase in a current density during pre-charging of the specimens causes a decrease in the thickness of twin plates, increases the density of twin boundaries and fraction of α'-martensite in the structure of the rolled specimens. The formation of a high density of $\Sigma 3^n$ boundaries (twin and ε-martensite) prevents the formation of a misoriented grain structure in austenite during rolling of steel specimens. Hydrogen pre-charging provides faster kinetics of γ→α' phase transformation in metastable steel AISI 321 during rolling.

Keywords: Austenitic stainless steel; Hydrogen; Twinning; Martensitic transformation; Microstructure

1. INTRODUCTION

The development of modern technologies places increasingly high demands on the performance properties of the iron-based alloys and, in particular, austenitic stainless steels. Steels of this class are a common structural material in the energy, chemical and food industries, the oil and gas extraction and transportation, and many other applications related to the human activity [1]. During operation, the individual constructional elements made of steel often interact with hydrogen-containing media. The problem of a hydrogen embrittlement (HE) has not yet been solved for austenitic stainless steels, although they are more resistant against HE in comparison, for example, with ferritic or martensitic steels [2,3].

The currently known hydrogen-affected behavior of metals, alloys and steels, and the HE models developed on its basis are diverse [4–7], but they are sometimes specific, trivial or contradictory. In modern literature, the following hydrogen-assisted behavior of austenitic stainless steels is most often mentioned: HE or, conversely, hydrogen-induced material plasticization, solid-solution hardening by hydrogen, hydrogen-enhanced twinning and phase transformations [6,8–14, and many other research papers]. As a rule, these effects were observed during experimental work under conditions of simple deformation schemes by uniaxial tension, where the strains before failure are relatively small [2,9,10,12,15]. Nevertheless, under conditions of a real loading of a three-dimensional structure, its stress state is much more complicated than that typical of uniaxial tension. Therefore, it is important to study the effect of hydrogen-charging on the structure and properties of austenitic steels under different deformation schemes.

There are not many works devoted to the severe plastic deformation of hydrogen-containing austenitic steels. For example, it was shown in [16,17] that hydrogen-saturation of AISI 304, 316L, and 310S steels can increase

* Corresponding author: Elena G. Astafurova, e-mail: elena.g.astafurova@ispms.ru

or decrease (depending on the hydrogen concentration) the volume content of deformation α'-martensite in them under high-pressure torsion. The mentioned research works do not give a complete picture of the effect of hydrogen on the regularities and mechanisms of martensitic transformations that occur during severe plastic deformation of austenitic CrNi steels. They also do not allow to unambiguously interpret the relationship of the hydrogen-assisted microstructure and the resulting physical and mechanical properties. In this regard, the effect of hydrogen-charging on the mechanisms of structural and phase transformations and the effect of the formed microstructure on the mechanical properties of austenitic steels during deformation by methods that allow achieving high strains remains open. The use of rolling for deformation of preliminarily hydrogen-charged samples looks attractive from the point of view of obtaining large-sized workpieces and studying their mechanical properties in comparison, for example, with the high-pressure torsion method used in [16,17]. Moreover, the high ductility and toughness of austenitic stainless steels make it possible to carry out their cold rolling to high strain (more than 90%) [1,18,19].

The primary objective of this paper is to establish the microstructure and phase transformations during rolling of hydrogen pre-charged samples of austenitic stainless steel type AISI 321.

2. MATERIALS AND METHODS

The chemical composition of the type AISI 321 steel is presented in Table 1. It was determined using a GD-Profiler HR emission glow discharge spectrometer (HORIBA Jobin Yvon, France). The billets with the linear dimensions 10×30×30 mm were cut from the industrially produced steel bars (hot-rolled) using electro-spark unit. Steel billets were solution-treated at 1100 °C for 1 h and quenched into water of room temperature. After solution treatment, steels have an austenitic structure with an average grain size of 15 μm (twin boundaries were excluded). Solution-treated materials were not textured.

From the solution-treated billets, the plain specimens for rolling with a gage section of 10×30×1.5 mm were cut using an electro-spark machining. They were cleaned by a chemical etching in a solution 2 parts HNO_3 + 3 parts HCl and mechanically grinded using sanding paper of different dispersion (the direction of the grinding was changed to perpendicular one on each sanding paper type). After mechanical grinding, an electrolytic polishing of the specimens in a supersaturated solution of chromium anhydride (CrO_3) in phosphoric acid (H_3PO_4) was performed (U = 25–30 V) until the mirror-like surface was obtained. Specimens (plates) prepared in this way had dimensions of 30×10×1 mm.

Table 1. Chemical compositions of the steel, Fe-balanced.

Element	Mass %
Cr	17.43
Ni	8.81
Mn	1.10
Si	0.42
Ti	< 0.5
C	0.08
N	< 0.01
S	< 0.02
P	< 0.03

Hydrogen pre-charging was conducted in a 1N H_2SO_4 solution (with a $CS(NH_2)_2$ as a recombination potion) at the current density of 10, 100 and 200 mA/cm^2 for 5 hours. After charging, hydrogen was distributed inhomogeneously, as we previously reported in Ref. [20]. Each specimen was put into the electrolytic bath between two plane electrodes (stainless steel), so both side surfaces were charged identically. As a result, surface layers of the specimens were saturated with hydrogen after charging. Such gradient distribution of hydrogen is typical for the electrochemical hydrogen saturation of the specimens, and it represents real industrial saturation of the material under cathodic protection of the steel constructions or corrosion [21]. Before rolling, hydrogen-charged specimens were kept in liquid nitrogen to suppress hydrogen diffusion and degassing. Hydrogen concentration was measured using Leco ONH spectrometer (Leco, USA).

Hydrogen-free and hydrogen pre-charged specimens were rolled at room temperature using a rolling mill with plain rollers (cold rolling – CR). The reduction was varied between 25 to 85%. After rolling, the hydrogen-affected microstructure of the steel was studied by a transmission electron microscopy (TEM, JEM-2100, JEOL, Tokyo Boeki Ltd., Tokyo, Japan). For TEM study, the specimens were mechanically grinded to the thickness of 0.2 mm. Thinning was performed from the different sides of the specimen to obtain the observation area in the 1/4 depth of the specimen (in the middle between central and surface parts of the specimens). Flat discs were cut from these thin foils and subjected to electropolishing in a solution of 95% glacial acetic acid (CH_3COOH) + 5% perchloric acid (H_3ClO_4). Indexing of selected area electron diffraction (SAED) patterns was performed as detailed elsewhere [22].

The average grain (subgrain) size d was determined as:

$$d = \Sigma d_i / n,$$

where d_i is the size of the i-th grain (subgrain), n is the number of measured grains.

The average width u of deformation twins (the projection width of twin plates on the foil plane) and the mean

distance e between twin boundaries were determined by the formulas:

$$u = \Sigma u_i / n \text{ and } e = \Sigma e_i / n,$$

where u_i is the thickness of the i-th twin, measured along the line perpendicular to its boundaries, e_i is the distance between the boundaries of adjacent twins, measured along a line perpendicular to its boundaries, n is the number of measured objects ($n > 30$).

The grain structure was investigated using the electron back scattered diffraction (EBSD) patterns obtained with scanning electron microscopes Quanta 200 3D and Quanta 600 FEG at an accelerating voltage of 30 kV with a step of 0.05÷0.15 μm. Kikuchi patterns formed by backscattered electrons were automatically indexed using the TSL OIM Data Collection software. The processing of data arrays obtained during scanning was carried out using the TSL OIM Analysis software. Data processing made it possible to obtain images (maps) of the grain-subgrain structure, the distribution of grain boundaries over misorientations, and to determine the linear density of twin boundaries:

$$\rho_{tw}^{EBSD} = \frac{(A \times B)}{(S \times E)},$$

where A is the fraction of 60° boundaries (twins), B is the length of all boundaries in the image, S is the area of the EBSD image, E is the fraction of the austenite phase.

X-ray studies were performed using a Shimadzu XRD-6000 diffractometer (with a monochromator) and Rigaku Ultima IV diffractometer using Cu Kα radiation in the angle range $2\theta = 40° \div 100°$ with a step of 0.02 degrees and exposure time at a point of 1 sec (with rotation of the specimen during the exposure). Samples with a surface parallel to the rolling plane were prepared for X-ray studies. To interpret X-ray patterns and qualitatively evaluate the phase ratio (α′-martensite and γ-austenite), a PowderCell 2.4 software and PDF (Powder Diffraction File) database were used.

Of the possible phases (γ, ε, α'), only the α' phase possesses ferromagnetism. The volume content of the magnetic α'-phase formed during the deformation of steels was determined by the ferritometer (MVP2, Kropus, Russia) and by the changing the specific magnetization depending on the magnetic field strength using the N-04 magnetometer (designed in Siberian Physical Technical Institute of Tomsk State University, Tomsk, Russia). The obtained dependences were recalculated into the volume content of the α'-phase ($V_{\alpha'}$):

$$V_{\alpha'} = \frac{\sigma_\alpha^{exp}}{\sigma_\alpha} \times 100\ \%,$$

where σ_α^{exp} is the specific magnetization measured experimentally, $\sigma_\alpha = 154$ G·cm^3/g is the specific magnetization of α'-martensite.

3. RESULTS

3.1. Structure and phase composition of the steel in the initial state

In the initial state, steel specimens had an average grain size of 15±10 μm (Fig. 1). X-ray diffraction analysis has shown that the initial steel structure (after solution treatment) is austenite with a lattice parameter of 3.592 Å. The ferrite was not revealed in the steel structure using the X-ray diffraction method. But magnetic phase analysis detects about 1% of the δ-ferrite in the solution-treated specimens. The proportion of high-angle boundaries (HABs) with a misorientation angle of more than 15° in the original samples is 95%, and 50% of them correspond to the special boundaries Σ3 (with a misorientation angle of 60°). The latter is due to the presence of annealing twins in the microstructure. The linear density of twin boundaries (annealing twins), determined by the EBSD analysis, is $\rho_{tw} = 0.09 \cdot 10^6$ m^{-1}. This parameter was introduced as an initial quantitative characteristic describing the deformation twin density in the microstructure of the steel specimens.

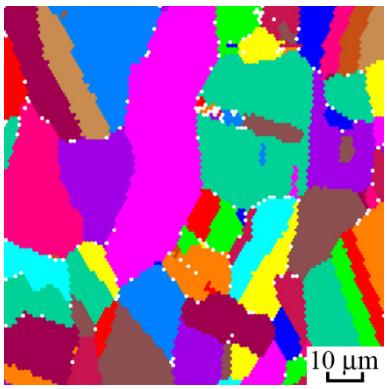

Fig. 1. EBSD grain map for the steel type AISI 321 in the solution-treated (initial) state.

3.2. Influence of CR on the microstructure and phase transformations of the hydrogen-free specimens

Rolling at room temperature affects the structure and phase composition of the steel. Severe plastic deformation promotes the refinement of the initially coarse austenitic grains down to the ultrafine-grained scale and is accompanied by phase transformation and accumulation of the crystal lattice defects of the different nature. A high density of slip dislocations ($\rho_{sl} \sim 10^{15}$ m^{-2}), deformation twins

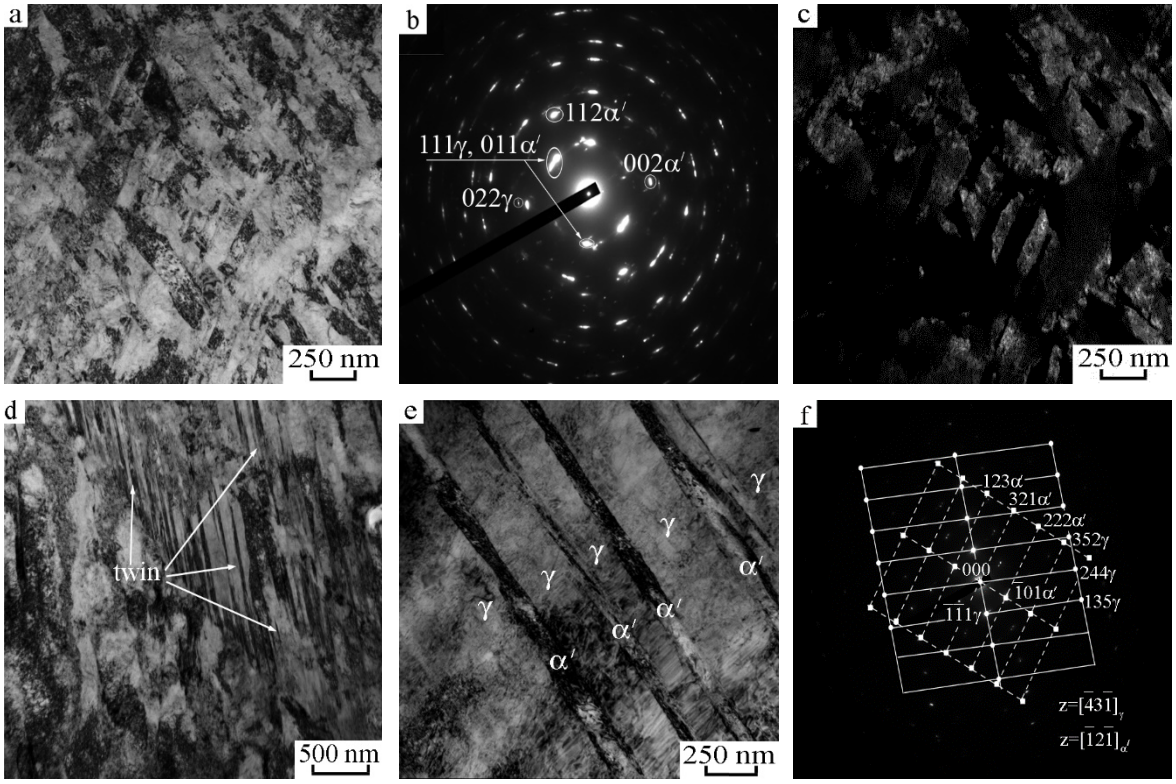

Fig. 2. TEM bright-field (a,d,e) and dark-field (c) images of the microstructure of AISI 321 steel after CR of hydrogen-free specimens. Images (b) and (f) are SAED patterns for (a) and (e), respectively. They were obtained from the areas 1.4 μm^2 and 0.5 μm^2, respectively. Image (c) was obtained in the combined reflections of the (111)γ and (110)α' phases. Rolling up to the 50% reduction.

and shear bands are formed in the steel microstructure. A detailed TEM analysis in this and next sections is given for an intermediate strain value (CR reduction of 50%).

Figure 2 shows TEM images of the steel microstructure after CR of hydrogen-free specimens. After CR with a reduction of 50%, rather homogeneous misoriented ultrafine-grained structure is formed in the most grains (Figs. 2a,d). SAED patterns (Fig. 2b) contain reflections both from the γ- and from the α'-phase. Therefore, CR of AISI 321 steel causes not only fragmentation of austenitic grains, but also the γ→α' phase transformation with the formation of deformation martensite in the microstructure. The average size of the structural elements is d = 150 nm (Fig. 2c). The d-value was determined from dark-field TEM images obtained in combined γ and α' reflections, so it represents (sub)grain size calculated taking into account both phases. The average (sub)grain size of α'-martensite ($d_{\alpha'}$) is 80 nm as determined using dark-field TEM images. These (sub)grains represent the fragments of the martensitic lamellas of different martensite variants (Fig. 2a). The formation of one variant of α'-martensite with lamellar morphology was also observed in some grains (Fig. 2e).

The SAED patterns obtained for the dual-phase (γ+α') misoriented structure in steel after CR include a set of reflections: a superposition of several zone axes, which is characteristic of misoriented polycrystalline states (Fig. 2b). Reflections have significant azimuthal diffusions, which indicates both low-angle misorientations and internal microstresses in the observation area of material. This is also confirmed by the data of the EBSD analysis: in Figure 3a there are areas that cannot be "identified" well (with low CI, confidence index).

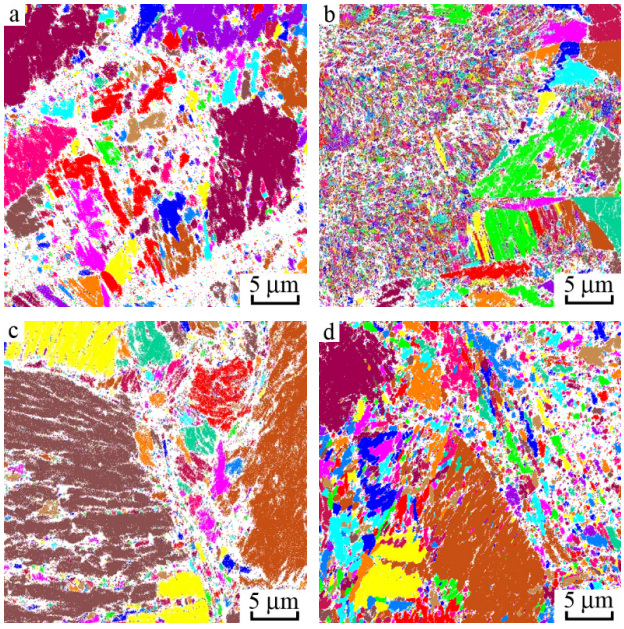

Fig. 3. EBSD grain maps. (a) CR of hydrogen-free specimens, (b–d) CR of hydrogen pre-charged specimens: (b) j = 10 mA/cm^2; (c) j = 100 mA/cm^2; (d) j = 200 mA/cm^2. CR up to the 50% reduction.

Despite the existence of the areas with "unsatisfactory" identification, which obviously correspond to the misoriented ultrafine-grained structure revealed by TEM, rather large fragments of austenitic grains with a size of ≈ 10 μm are visible on the EBSD maps (Fig. 3a). In such areas the accumulation of dislocations, deformation twins, lamellas of α'-martensite takes place under CR with 50% reduction but ultrafine-grained structure has not been formed yet.

Typical bright-field TEM images of microstructure regions with rather large fragments of the austenitic structure, twins and lamellas of α'-martensite in them are shown in Figures 2d and 2e. Twin and martensitic lamellas in such austenitic fragments are distorted and fragmented. The thickness of the individual twins in twin packets is in the range $u = 15 \div 25$ nm, and the distance between them is $e = 25 \div 50$ nm (Fig. 2d). According to EBSD-analysis, linear density of special (twin) boundaries is $\rho_{tw}^{EBSD} = 0.57 \times 10^6$ m^{-1}, that is, it is six times higher than in the initial solution-treated state (Table 2). Due to the limitation in resolution of EBSD analysis relative to the TEM, it gives an underestimated value of ρ_{tw}^{EBSD} because only the boundaries of twin packets with a thickness of more than tens of nanometers can be visualized and identified correctly. While thinner twin lamellas that are part of twin packets are not detected. TEM analysis provides more correct data on the parameters of deformation twins (Table 3), but it is difficult to estimate their density due to the heterogeneity of the structure at the mesoscale.

XRD and magnetic phase analysis of the specimens confirm the data obtained by TEM and EBSD methods on the occurrence of the γ→α' phase transformation with the formation of a significant fraction of deformation martensite in the steel structure. XRD lines for ε-martensite were not observed on XRD patterns (also not detected by TEM studies). That is, no ε martensite forms during the CR of AISI 321 steel and the γ→α' phase transformation is realized without the formation of an intermediate ε-phase. This correlates well with the characteristics of martensitic transformations in chromium-nickel austenitic steels published earlier in [23,24]. The deformation martensite forms from the very beginning of CR, and with an increase in strain, the volume fraction of the α'-phase increases monotonically (data on the kinetics of martensitic transformation will be analyzed in Section 3.4).

The performed analysis indicates the following sequence of structural and phase transformations in AISI 321 steel during rolling of hydrogen-free specimens. In the process of deformation, a high density of dislocations is accumulated, and the initial austenitic grains are fragmented due to multiple slip activity, deformation twinning and γ→α' martensitic transformation. The deformation conditions during rolling (stress state) contribute to a rather rapid fragmentation of grains: the formation of twin lamellas, localized deformation bands, (sub)grains of the α'-phase (lamellas), and the formation of subboundaries of a dislocation nature. As a result, the ultrafine-grained structure is formed, which contains both low-angle, high-angle and interphase boundaries. These data confirm the previously described regularities of grain refinement for metastable austenitic chromium-nickel steels subjected to severe deformation by rolling [23], high-pressure torsion [25], and equal channel angular pressing [26].

Table 2. Linear density of twin boundaries (ρ_{tw}^{EBSD}) in the specimens of AISI 321 steel before and after CR up to 50% reduction. Data obtained by EBSD method.

Treatment	ρ_{tw}^{EBSD}, m^{-1}
Initial	0.09×10^6
CR	0.57×10^6
j = 10 mA/cm^2 + CR	1.82×10^6
j = 100 mA/cm^2 + CR	2.20×10^6
j = 200 mA/cm^2 + CR	0.81×10^6

3.3. Influence of CR on the microstructure and phase transformations of the hydrogen pre-charged specimens

Figure 4 shows TEM images of the steel microstructure after hydrogen pre-charging at current density j = 10 mA/cm^2 and subsequent CR with reduction of 50%. This treatment leads to the formation of an oriented structure consisting of

Table 3. Characteristics of steel microstructure after CR: d is the average size of structural elements, $d_{\alpha'}$ and d_γ are the average (sub)grain sizes of the α'-phase and γ-phase, ρ_{disl} is the dislocation density, u is the thickness of twins, e is the distance between twins. In the right column, the data about the presence of ε and α'-martensite are given ("+" is observed, "–" is not observed). Reduction is 50%. Data obtained by TEM method.

Treatment	d, nm	ρ_{disl}, m^{-2}	$d_{\alpha'}$, nm	γ-phase			ε-phase / α'-phase
				d_γ, nm	u, nm	e, nm	
CR	150	1.3×10^{15}	80	–	15÷25	25÷50	–/+
j = 10 mA/cm^2 + CR	230	1.3×10^{15}	85	–	5÷10	13÷15	+/+
j = 100 mA/cm^2 + CR	210	0.8×10^{15}	90	130	1÷10	5÷15	+/+
j = 200 mA/cm^2 + CR	230	0.8×10^{15}	110	290	10÷15	10÷15	+/+

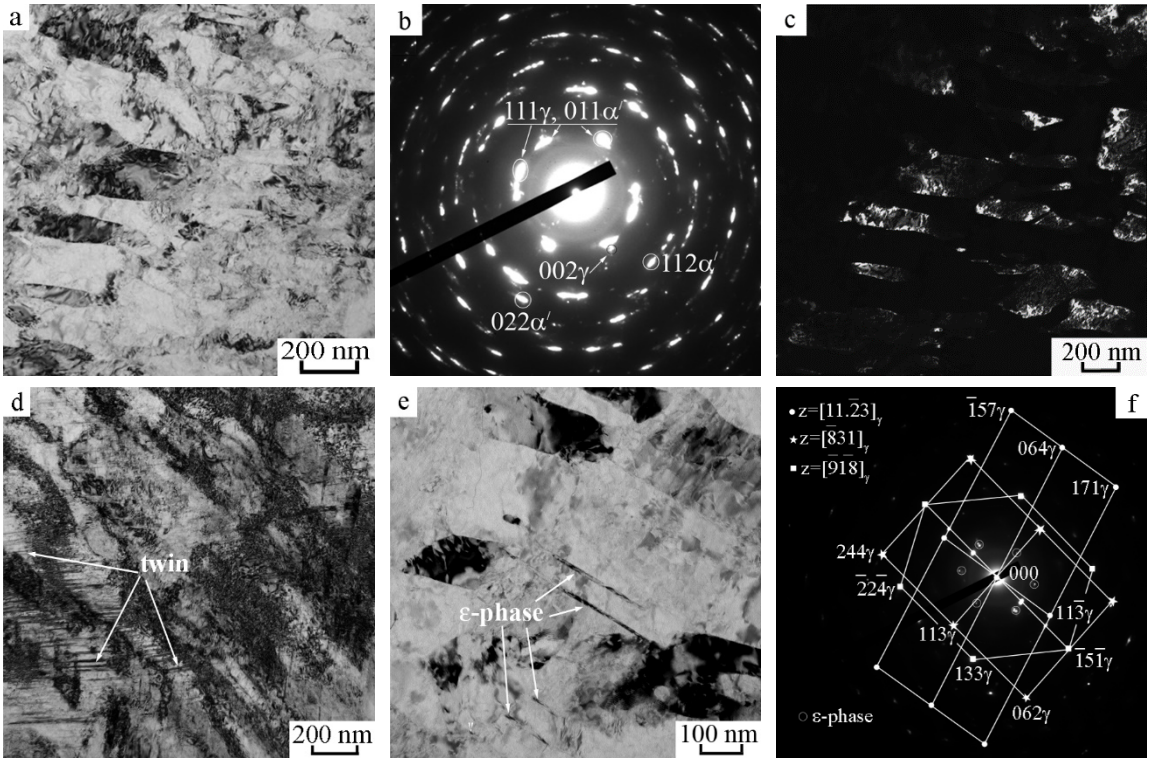

Fig. 4. TEM bright-field (a,d,e) and dark-field (c) images of the microstructure of AISI 321 steel after pre-charging at j = 10 mA/cm^2 and CR. Images (b) and (f) are SAED patterns for (a) and (e), respectively. Image (c) was obtained in the combined reflection of γ and α'-phase. SAED patterns (b) and (f) were taken from an area of 1.4 μm^2 and 0.5 μm^2, respectively. CR up to the 50% reduction.

elongated non-equiaxed grains and subgrains (Fig. 4a). The linear dimensions of the elements of the (sub)grain structure vary in the range of 200÷350 nm, and the average value is d = 230 nm (averaged for both phases) as it has been determined from dark-field TEM analysis. The SAED patterns are of a quasi-ring nature (Fig. 4b), which indicates a greater proportion of the high-angle boundaries in the steel structure as compared to CR without hydrogen pre-charging. Significant azimuthal diffusions of the reflections indicate the presence of high internal stresses and low-angle continuous misorientations in the microstructure. In addition to γ- and α'-phases, thin plates of twins and ε-phase in austenite grains were observed (Figs. 4e,f). On SAED pattern obtained for a sufficiently large area (Fig. 4b), diffuse rings with interplanar spacings corresponding to ε-martensite are visible. This confirms the high dispersion of this phase.

After 50% reduction by CR, combined with hydrogen pre-charging at current densities of 100 and 200 mA/cm^2, the structure of AISI 321 steel is even more inhomogeneous than those corresponding to the specimens treated at j = 10 mA/cm^2 or rolled in hydrogen-free state (Figs. 3a–d, 4a, 5a). Figure 5 represents TEM images for specimens pre-charged at j = 100 mA/cm^2 before CR; for j = 200 mA/cm^2, the microstructure is qualitatively similar. Along with the ultrafine-grained (γ+α') dual-phase structure, large austenitic grains with a high density of twin boundaries and ε-phase are observed (Figs. 3c,d, 5e, 5f). The SAED patterns are of a quasi-ring nature from regions with misoriented γ+α' ultrafine-grained structure and ε-phase (Fig. 5b). Along with the quasi-ring distribution of the reflections, SAED patterns simultaneously contain intensive point reflections from the austenitic phase, which correspond to the single zone axis and have diffusions typical of twinning and γ→ε transformation (Fig. 5b). It should be noted that ε-martensite plates are quite rare in the structure of the studied specimens compared to α'-martensite and deformation twins.

For steels with low stacking fault energy (SFE) (or at low-temperature deformation, when the SFE decreases), the γ→ε→α' phase transformation is accompanied first by an increase in the volume fraction of ε-martensite, and then (at high strain values) the fraction of α'-phase increases, while the content of the ε-phase decreases [27,28]. X-ray analysis does not reveal ε-martensite (it was also not observed at lower degrees of reduction, Figure 6). The above data of XRD, TEM and EBSD indicate that hydrogen pre-charging does not change the sequence of the phase transformation from γ→α' to γ→ε→α'. And γ→ε-martensitic transformation develops with very slow kinetics during CR in addition to the main γ→α' phase transformation. That is, hydrogen charging contributes to the development of a series of phase transformations in AISI 321 steel during CR: deformation of specimens without hydrogen pre-charging is accompanied by the γ→α' transformation, and

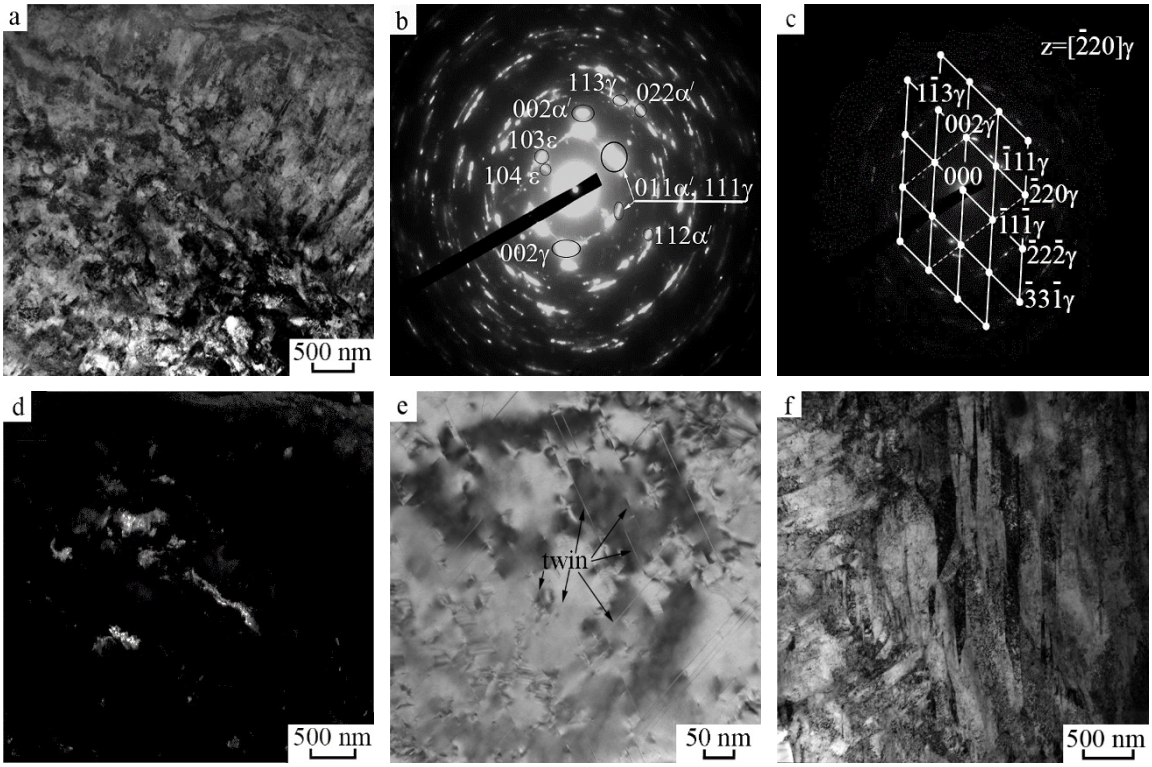

Fig. 5. TEM bright-field (a,e,f) and dark-field (d) images of the microstructure of AISI 321 steel after pre-charging at j = 100 mA/cm^2 and CR. Images (b,c) are SAED patterns to (a); they were taken from the areas of 1.4 μm^2 and 0.5 μm^2, respectively. In (c), the traces of twin planes are indicated by the dotted lines. Image (d) was obtained in the reflection of the α'-phase. Rolling up to 50% reduction.

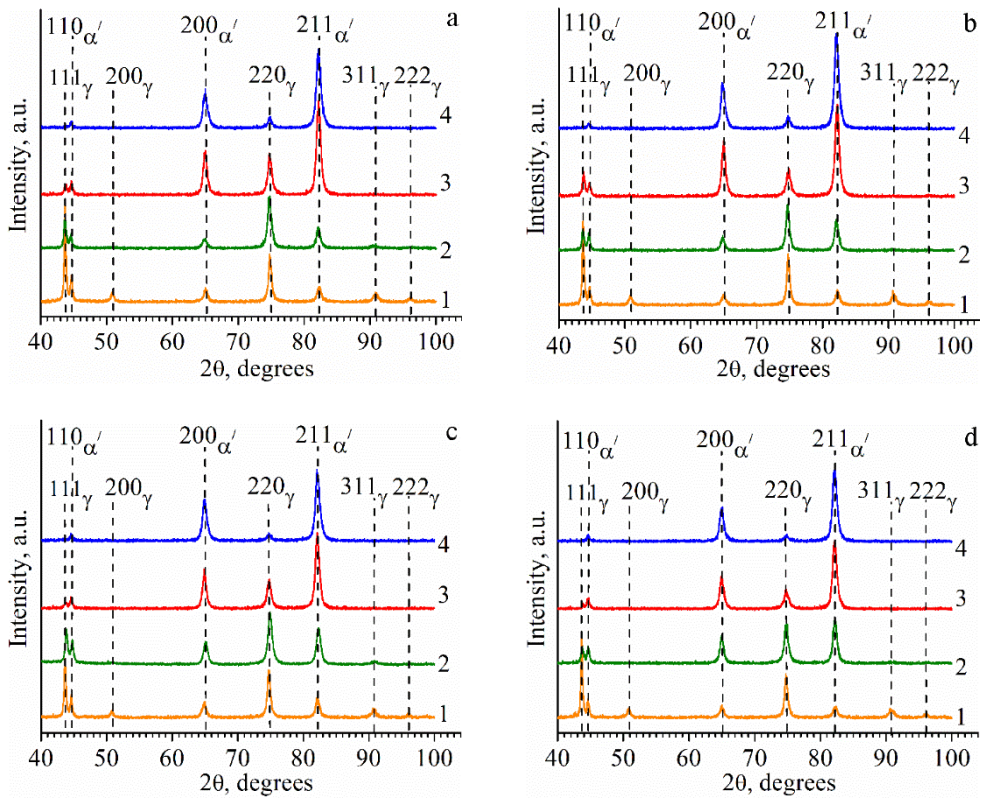

Fig. 6. XRD patterns for steel specimens after rolling in hydrogen-free (a) and hydrogen precharged (b–d) states: (b) j = 10 mA/cm^2; (c) j = 100 mA/cm^2; (d) j = 200 mA/cm^2. Reduction ratio: (1) – 25%, (2) – 50%, (3) – 75%, (4) – 85%.

during CR of hydrogen pre-charged specimens the γ→ε martensitic transformation is also realized in addition to the main γ→α' one. In Ref. [8], the appearance of deformation γ→ε-martensitic transformation was observed during uniaxial tension of hydrogen-charged specimens of AISI 321 steel, and the formation of ε-martensite was associated with a hydrogen-assisted decrease in the SFE of austenite.

According to TEM data, the frequency of detection of austenitic fragments, in which deformation twins are observed, is significantly higher than in the case of rolling of hydrogen-free steel. EBSD-analysis confirms that preliminary hydrogen charging of steel specimens contributes to an increase in fraction of Σ3 boundaries and an increase in the linear density of twin boundaries in austenite during CR (Table 2). The data of the EBSD-analysis in Table 2 should be treated with caution and used only for qualitative analysis. Nevertheless, the arguments about the increase in the contribution of mechanical twinning to the formation of the structure due to hydrogen charging prior to rolling are justified. According to the EBSD-analysis, the linear density of twin boundaries decreases with increasing current density during the hydrogen-precharging. However, the EBSD method makes it possible to identify twins with a width of more than ≈ 60 nm, and during TEM studies, deformation twins with a lamella thickness u = 1÷15 nm and an average distance between twins e = 5÷15 nm were observed (Table 3). But even despite this fact, the density of twin boundaries, determined using EBSD-analysis, is higher for specimens rolled after hydrogen pre-charging. Hydrogen-assisted activation of deformation twinning and the ε-phase correlates well with the data of Refs. [8,29,30] on the hydrogen-induced decrease in the SFE of steel, since the stresses for twinning are inversely proportional to the SFE value. And the hydrogen-induced enhancement of twinning favorably affects the tendency of steel to γ→α' transformation. In this case, the γ→t→α' transition (t is twinning) plays an important role [31].

The formation of a high density of twin boundaries in austenitic grains prevents the formation of a misoriented grain structure due to the difficulty of transferring plastic shear through the coherent boundary of a "thin" twin, as was shown earlier in works on severe plastic deformation of TWIP steels (TWinning Induced Plasticity) [32]. Since an increase in the current density during hydrogen precharging contributes to the formation of twins with thinner plates, this causes the experimentally observed inhomogeneity of the structure at the mesoscale—rather large areas of austenite with twins are observed in the structure, in which the formation of subboundaries of dislocation origin is hindered. Twins and ε-martensite are not formed immediately in all grains due to the existence of the orientational dependence of this deformation mechanism [33,34]. Therefore, in those grains where the development of twinning is "difficult", the formation of a misoriented grain-subgrain structure occurs.

Thus, the electron microscopic analysis of the phase composition and microstructure of hydrogen pre-charged and rolled specimens showed that hydrogen charging enhances the contribution of mechanical twinning to the fragmentation of the steel structure and promotes the formation of ε-martensite. Both factors cause an increase in the proportion of high-angle special boundaries and contribute to the formation of α'-martensite in the steel structure during rolling. An increase in the current density during hydrogen charging of AISI 321 steel specimens before deformation causes a decrease in the thickness of twin plates and, accordingly, increases the density of twin boundaries in the structure of rolled specimens, which also contributes to the transformation.

3.4. Influence of hydrogen pre-charging on the kinetics of the γ→α' phase transformation

XRD patterns for specimens subjected to different processing modes are shown in Figure 6. The XRD patterns for the rolled specimens contain lines with interplanar spacings corresponding to the γ- and α'-phases. With an increase in strain during CR and current density during hydrogen pre-charging, the values of the parameters of the crystal lattice of both phases change withing a measurement error. The ratio of X-ray lines at different strains indicates the formation of texture in the rolled specimens.

Kinetic curves describing the change in the fraction of α'-martensite depending on the true strain for steel specimens after different deformation regimes are shown in Figure 7. Regardless of the current density during hydrogen pre-charging, when the strain value reaches 85%, the steel structure consists predominantly of the α'-phase (95÷99%).

Data in Figure 7a shows that the hydrogen pre-charging changes the kinetics of the deformation phase transformation during rolling of the steel. The analytical description of the martensitic transition kinetics in recent theoretical works takes into account a large number of parameters and their change during deformation (dislocation density, deformation bands, twinning, frequency of formation of nuclei of α'- and ε-martensite, etc.) [27,28,35]. In this work, we describe the change in the transformation kinetics using the basic ratios for modified Olson-Cohen model and sigmoid relation [36]:

$$\frac{V_{\alpha'}}{V_{\alpha'}^{\infty}} = \left(1 + \frac{e^{-B}}{A}\right)^{-1}, \tag{1}$$

$$\frac{V_{\alpha'}}{V_{\alpha'}^{\infty}} = 1 - \exp(-ke^{m}). \tag{2}$$

Here $V_{\alpha'}$ is the volume fraction of martensite, $V_{\alpha'}^{\infty}$ is the asymptotic value of $V_{\alpha'}$ at $e \to \infty$, e is the true strain (during rolling $e = (2/\sqrt{3})\ln(h_i / h_f)$, where h_i and h_f are the initial and final plate thicknesses), k, m, A, B are constants. These analytical dependences are not based on any specific model ideas about the nucleation of martensite, the defect structure of austenite, and other structural parameters, but they qualitatively correctly describe the different stages of transformation observed in the paper for hydrogen-free and hydrogen pre-charged specimens during rolling. For the case of rolling of hydrogen-free specimens, the kinetics is qualitatively correctly described by equation (1) with the following parameters (Fig. 8b):

$V_{\alpha'}^{\infty} = 100\%$, $A = 1.04$, $B = 0.87$,

that is

$$V_{\alpha'} = \frac{100\%}{1 + 0.95 \cdot e^{-0.87}} \approx \frac{e}{1+e} \cdot 100\%.$$

For the case of rolling of hydrogen pre-charged specimens at $j = 200$ mA/cm^2, the kinetics of the transformation is described with high accuracy by equation (2) with the following parameters:

$V_{\alpha'}^{\infty} = 99.4\%$, $k = 1.5$, $m = 1$,

that is

$$V_{\alpha'} = (1 - \exp(-1.5e)) \cdot 99.4\% \approx (1 - \exp(-\frac{3}{2}e)) \cdot 100\%.$$

The above data on the kinetics of the phase transformations and the data of micro-structural analysis indicate that hydrogen stimulates the γ→α' transformation. The intensity of the transformation (increment of the relative fraction of the α'-phase per unit of strain) is higher in specimens with hydrogen, and it increases with increasing current density during hydrogen pre-charging (Fig. 7a). In other words, at a fixed strain (25, 50, 75%), the transformation in specimens with hydrogen is more complete.

The concentration of hydrogen atoms in the specimens immediately after charging for 5 h is 30 ppm and it weakly depends on j-value. At first glance, this result looks unexpected, since the concentration of ionized hydrogen in the electrolyte near the surface of the saturable specimen during saturation increases with increasing j. But in this work we use electrochemical charging with high values of $j = (10 \div 200)$ mA/cm^2, when we are in the saturation regime on the $C_H(j)$ dependence. The hydrogen charging of the specimens is determined by the diffusion of hydrogen along the grain boundaries and in the crystal lattice of the austenitic phase, that is, the effective diffusion coefficient. It has a finite value. After 5 h of hydrogen pre-charging, hydrogen diffuses to a depth of no more than 5 μm, regardless of the current density, and is found only in the surface layer of the specimens [20]. An increase in the hydrogen concentration at the saturating surface can lead to the activation of the so-called "skin effect" [37], which consists in "blocking" the diffusion of hydrogen into the specimen, provided that its concentration in the surface layer of the specimen becomes excessively high. With the accumulation of the same total hydrogen concentration in the surface layers at different j, the observed differences in the phase transformation kinetics for the considered specimens indicate the formation of different hydrogen distribution profiles in the surface layers of the samples saturated with hydrogen. The mechanisms that determine these processes require detailed research in the framework of independent work. But it can be said that for specimens saturated with hydrogen at $j = 200$ mA/cm^2, the hydrogen concentration near the surface can be higher than for saturated at lower current densities, that is, the depth distribution profile of hydrogen is steeper.

If we consider the entire specimen as a set of volumes of small thickness ΔV (layers parallel to the saturation sur-

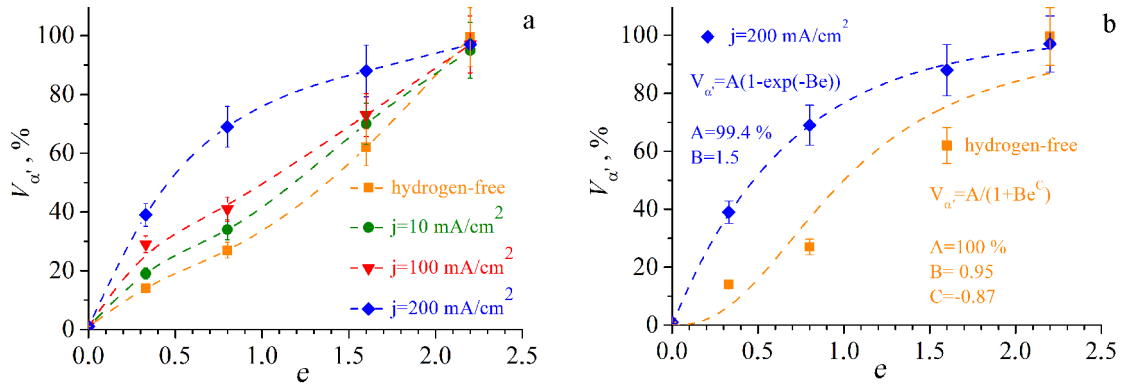

Fig. 7. The fraction of the α'-phase ($V_{\alpha'}$) vs. true strain (e) for the steel specimens subjected to the CR after hydrogen pre-charging (the charging regimes are indicated on the diagrams): (a) experimental data for all regimes, (b) approximation of experimental data by equations (1) and (2), for specimens rolled without hydrogen pre-charging and after hydrogen-charging at $j = 200$ mA/cm^2.

face with thickness $\Delta l \to 0$), then as a result of the load application during rolling, in n surface layers containing a high concentration of hydrogen, twinning, deformation localization, and nucleation of martensite are actively developed. During rolling, hydrogen-induced twinning and γ→ε martensitic transformations and the formation of the α'-phase in the material develop as a self-organizing process. The diffusion mobility of hydrogen in ferrite is significantly higher than in the austenitic phase: $D_\gamma = (1.4 \div 8.0) \cdot 10^{-16}$ m^2/s and $D_\alpha \sim 10^{-10} \div 10^{-12}$ m^2/s at room temperature [38,39]. Therefore, the martensite lamellas formed in the surface layers of thickness $n\Delta l$ act as diffusion channels for hydrogen into deeper layers of the material [40]. Further, in the next volume of the austenitic phase from the surface, hydrogen again stimulates twinning and the formation of the α'-phase, and the process is repeated until it successively spreads over the entire thickness of the specimen. The process has a dynamic nature since during rolling a high strain rate and high stresses are realized—all these factors contribute to the diffusion of hydrogen, the development of twinning and martensitic transformations, along with the hydrogen-induced decrease in the SFE and the facilitation of dislocation slip, dislocation annihilation, and microlocalization processes (HELP effect [4,6,41]). During saturation at lower current densities, the hydrogen distribution profile is flatter, the hydrogen concentration near the surface is lower, and the transformation intensity (the tendency to twinning and microlocalization) is lower, which determines the slower kinetics of the deformation phase transformation.

4. CONCLUSIONS

The effect of hydrogen pre-charging (in a 1N H_2SO_4 solution with a $CS(NH_2)_2$ as a recombination potion, at the current densities of 10, 100 and 200 mA/cm^2, for 5 hours) on the microstructure and phase transformations of a type AISI 321 austenitic stainless steel during room-temperature rolling has been investigated. The main results can be summarized as following:

1. A hydrogen-assisted change in the kinetics of deformation γ→α' martensitic transformation during rolling has been experimentally confirmed for metastable austenitic steel. Deformation induced phase transformation is realized more completely and with the higher intensity in steel specimens, which were hydrogen pre-charged before cold rolling.

2. Hydrogen-charging contributes to a more active development of mechanical twinning and stimulates γ→ε martensitic transformation during rolling of metastable steel type AISI 321.

3. Preliminary hydrogen-charging of the type AISI 321 steel specimens assists the formation of a high density of special boundaries $\Sigma 3^n$ (twin and ε-martensite) during rolling, which prevents the formation of a misoriented structure in austenite with the formation of low-angle and high-angle boundaries of dislocation origin.

ACKNOWLEDGMENTS

This research was funded by the Government research assignment for ISPMS SB RAS, project FWRW-2022-0005. The study was conducted using the equipment of ISPMS SB RAS ("Nanotech" center) and center for collective use "Diagnostics of the Structure and Properties of Nanomaterials" (Belgorod State University).

REFERENCES

[1] K.H. Lo, C.H. Shek, J.K.L. Lai, Recent developments in stainless steels, *Mater. Sci. Eng. R*, 2009, vol. 65, no. 4–6, pp. 39–104.
[2] T. Michler, C. San Marchi, J. Naumann, S. Weber, M. Martin, Hydrogen environment embrittlement of stable austenitic steels, *Int. J. Hydr. Energy*, 2012, vol. 37, no. 21, pp. 16231–16246.
[3] R.A. Oriani, A mechanistic theory of hydrogen embrittlement of steels, *Ber. Bunsengesellsch. Phys. Chem.*, 1972, vol. 76, no. 8, pp. 848–857.
[4] M. Nagumo, *Fundamentals of hydrogen embrittlement*, Springer, Singapore, 2016.
[5] S. Lynch, Hydrogen embrittlement phenomena and mechanisms, *Corros. Rev.*, 2012, vol. 30, no. 3–4, pp. 105–123.
[6] H.K. Birnbaum, P. Sofronis, Hydrogen-enhanced localized plasticity–a mechanism for hydrogen-related fracture, *Mater. Sci. Eng. A*, 1994, vol. 176, no. 1–2, pp. 191–202.
[7] P.J. Ferreira, I.M. Robertson, H.K. Birnbaum, Hydrogen effects on the character of dislocations in high-purity aluminium, *Acta Mater.*, 1999, vol. 47, no. 10, pp. 2991–2998.
[8] P. Rozenak, L. Levin, D. Eliezer, Hydrogen effects on phase transformations in austenitic stainless steels, *J. Mater. Sci.*, 1984, vol. 19, no. 2, pp. 567–573.
[9] E.G. Astafurova, E.V. Melnikov, S.V. Astafurov, I.V. Ratochka, I.P. Mishin, G.G. Maier, V.A. Moskvina, G.N. Zakharov, A.I. Smirnov, V.A. Bataev, Hydrogen embrittlement effects on austenitic stainless steels with ultrafine-grained structure of different morphology, *Phys. Mesomech.*, 2019, vol. 22, pp. 313–326.
[10] J. Morisawa, M. Kodama, S. Nishimura, K. Asano, K. Nakata, S. Shima, Effects of hydrogen on mechanical properties in irradiated austenitic stainless steels, *J. Nuclear Mater.*, 1994, vol. 212–215, pp. 1396–1400.
[11] L.R. Queiroga, G.F. Marcolino, M. Santos, G. Rodrigues, C. Eduardo dos Santos, P. Brito, Influence of machining parameters on surface roughness and susceptibility to hydrogen embrittlement of austenitic stainless steels, *Int. J. Hydr. Energy.*, 2019, vol. 44, no. 54, pp. 29027–29033.
[12] S. Weber, M. Martin, W. Theisen, Impact of heat treatment on the mechanical properties of AISI 304L austenitic stainless steel in high-pressure hydrogen gas, *J. Mater. Sci.*, 2012, vol. 47, no. 16, pp. 6095–6107.
[13] D.P. Abraham, C.J. Altstetter, The effect of hydrogen on the yield and flow stress of an austenitic stainless steel,

Metall. Mater. Trans. A, 1995, vol. 26, no. 11, pp. 2849–2858.

[14] D.P. Abraham, C.J. Altstetter, Hydrogen-enhanced localization of plasticity in an austenitic stainless steel, *Metall. Mater. Trans. A*, 1995, vol. 26, no. 11, pp. 2859–2871.

[15] M. Koyama, E. Akiyama, T. Sawaguchi, K. Ogawa, I.V. Kireeva, Y.I. Chumlyakov, K. Tsuzaki, Hydrogen assisted quasi-cleavage fracture in a single crystalline type 316 austenitic stainless steel, *Corros. Sci.*, 2013, vol. 75, pp. 345–353.

[16] Y. Mine, Z. Horita, Y. Murakami, Effect of hydrogen on martensite formation in austenitic stainless steels in high-pressure torsion, *Acta Mater.*, 2009, vol. 57, no. 10, pp. 2993–3002.

[17] Y. Mine, C. Narazaki, K. Murakami, S. Matsuoka, Y. Murakami, Hydrogen transport in solution-treated and pre-strained austenitic stainless steels and its role in hydrogen-enhanced fatigue crack growth, *Int. J. Hydr. Energy*, 2009, vol. 34, no. 2, pp. 1097–1107.

[18] A.F. Padilha, R.L. Plaut, P.R. Rios, Annealing of cold-worked austenitic stainless steels. *ISIJ Int.*, 2003, vol. 43, no. 2, pp. 135–143.

[19] V. Shrinivas, S.K. Varma, L.E. Murr, Deformation-induced martensitic characteristics in 304 and 316 stainless steels during room-temperature rolling, *Metall. Mater. Trans. A*, 1995, vol. 26, no. 3, pp. 661–671.

[20] E. Astafurova, A. Fortuna, E. Melnikov, S. Astafurov, The effect of strain rate on hydrogen-assisted deformation behavior and microstructure in AISI 316L austenitic stainless steel, *Materials*, 2023, vol. 16, no. 8, art. no. 2983.

[21] Y. Yagodzinskyy, O. Todoshchenko, S. Papula, H. Hänninen, Hydrogen solubility and diffusion in austenitic stainless steels studied with thermal desorption spectroscopy, *Steel Res. Int.*, 2011, vol. 82, no .1, pp. 20–25.

[22] D.B. Williams, C.B. Carter, *Transmission Electron Microscopy. Textbook for Materials Science*, Springer, New York, USA, 2009.

[23] I. Shakhova, V. Dudko, A. Belyakov, K. Tsuzaki, R. Kaibyshev, Effect of large strain cold rolling and subsequent annealing on microstructure and mechanical properties of an austenitic stainless steel, *Mater. Sci. Eng. A*, 2012, vol. 545, pp. 176–186.

[24] C. Donadille, R. Valle, P. Dervin, R. Penelle, Development of texture and microstructure during cold-rolling and annealing of f.c.c. alloys: example of an austenitic stainless steel, *Acta Metall.*, 1989, vol. 37, no. 6, pp. 1547–1571.

[25] O.V. Rybalchenko, D.V. Prosvirnin, A.A. Tokar, V.P. Levin, M.R. Tyutin, G.I. Raab, L.R. Botvina, S.V. Dobatkin, Effect of ECAP on structural, mechanical and functional characteristics of the austenitic Cr-Ni-Ti steels, *J. Phys.: Conf. Ser.*, 2018, vol. 1134, art. no. 012049.

[26] S.V. Dobatkin, O.V. Rybalchenko, N.A. Enikeev, A.A. Tokar, M.M. Abramova, Formation of fully austenitic ultrafine-grained high strength state in metastable Cr–Ni–Ti stainless steel by severe plastic deformation, *Mater. Lett.*, 2016, vol. 166, pp. 276–279.

[27] A.K. De, J.G. Speer, D.K. Matlock, D.C. Murdock, M.C. Mataya, R.J. Comstock, Deformation-induced phase transformation and strain hardening in type 304 austenitic stainless steel, *Metal. Mater. Trans. A*, 2006, vol. 37, no. 6, pp. 1875–1886.

[28] E.I. Galindo-Nava, P.E.J. Rivera-Díaz-del-Castillo, Understanding martensite and twin formation in austenitic steels: A model describing TRIP and TWIP effects, *Acta Mater.*, 2017, vol. 128, pp. 120–134.

[29] C. Zhang, H. Zhi, S. Antonov, L. Chen, Y. Su, Hydrogen-enhanced densified twinning (HEDT) in a twinning-induced plasticity (TWIP) steel, *Scr. Mater.*, 2021, vol. 190, pp. 108–112.

[30] M. Koyama, N. Terao, K. Tsuzaki, Revisiting the effects of hydrogen on deformation-induced γ-ε martensitic transformation, *Mater. Lett.*, 2019, vol. 249, pp. 197–200.

[31] J.S. Aristeidakis, G.N. Haidemenopoulos, Constitutive and transformation kinetics modeling of ε-, α′-martensite and mechanical twinning in steels containing austenite. *Acta Mater.*, 2022, vol. 228, art. no. 117757.

[32] E.G. Astafurova, M.S. Tukeeva, G.G. Maier, E.V. Melnikov, H.J. Maier, Microstructure and mechanical response of single-crystalline high-manganese austenitic steels under high-pressure torsion: The effect of stacking-fault energy, *Mater. Sci. Eng. A*, 2014, vol. 604, pp. 166–175.

[33] I.V. Kireeva, Y.I. Chumlyakov, Effect of nitrogen and stacking-fault energy on twinning in $[\bar{1}11]$ single crystals of austenitic stainless steels, *Phys. Metals Metallogr.*, 2009, vol. 108, no. 3, pp. 298–309.

[34] I.V. Kireeva, Y.I. Chumlyakov, Orientation dependence of the γ-ε martensitic transformation in single crystals of austenitic stainless steels with low stacking fault energy, *Phys. Metals Metallogr.*, 2006, vol. 101, no. 2, pp. 186–203.

[35] X.-S. Yang, S. Sun, T.-Y. Zhang, The mechanism of bcc α′ nucleation in single hcp ε laths in the fcc γ → hcp ε → bcc α′ martensitic phase transformation, *Acta Mater.*, 2015, vol. 95, pp. 264–273.

[36] M.J. Sohrabi, M. Naghizadeh, H. Mirzadeh, Deformation-induced martensite in austenitic stainless steels: A review, *Archiv. Civ. Mech. Eng.*, 2020, vol. 20, no. 4, art. no. 124.

[37] V.A. Polyanskiy, A.K. Belyaev, E.L. Alekseeva, A.M. Polyanskiy, D.A. Tretyakov, Yu.A. Yakovlev, Phenomenon of skin effect in metals due to hydrogen absorption, *Continuum Mech. Thermodyn.*, 2019, vol. 31, no. 6, pp. 1961–1975.

[38] E. Owczarek, T. Zakroczymski, Hydrogen transport in a duplex stainless steel, *Acta Mater.*, 2000, vol. 48, no. 12, pp. 3059–3070.

[39] V. Olden, C. Thaulow, R. Johnsen, Modelling of hydrogen diffusion and hydrogen induced cracking in supermartensitic and duplex stainless steels, *Mater. Des.*, 2008, vol. 29, no. 10, pp. 1934–1948.

[40] H. Zhan, Y. Li, W. Liang, L. Zheng, Observation of diffusion channel and hydrogen trap in 304 austenitic stainless steel, *Mater. Lett.,* 2021, vol. 290, art. no. 129453.

[41] I.M. Robertson, The effect of hydrogen on dislocation dynamics, *Eng. Fra. Mech.*, 2001, vol. 68, no. 6, pp. 671–692.

УДК 538.91

Водородно-индуцируемые мартенситные превращения и двойникование в аустенитной нержавеющей стали AISI 321 при прокатке

Е.Г. Астафурова, Е.В. Мельников, С.В. Астафуров

Лаборатория физики иерархических структур в металлах и сплавах, Институт физики прочности и материаловедения СО РАН, Академический пр., 2/4, Томск, 634055, Россия

Аннотация. Исследовано влияние электролитического насыщения водородом (в растворе 1N H_2SO_4 с добавлением $CS(NH_2)_2$, при плотностях тока 10, 100 и 200 мА/см^2 в течение 5 часов) на микроструктуру и фазовый состав аустенитной нержавеющей стали AISI 321 во время прокатки при комнатной температуре. Экспериментально показано, что насыщение стальных образцов водородом усиливает вклад механического двойникования в фрагментацию их структуры и способствует реализации γ→α' и γ→ε превращений во время прокатки. Как двойникование, так и мартенситные превращения зависят от режима наводороживания: увеличение плотности тока при насыщении образцов водородом вызывает уменьшение толщины двойниковых пластин, увеличивает плотность двойниковых границ и долю α'-мартенсита в структуре прокатанных образцов. Образование высокой плотности границ $\Sigma 3^n$ (двойниковых и мартенситных) препятствует образованию разориентированной зеренной структуры в аустените при прокатке стальных образцов. Показано, что предварительное насыщение водородом обеспечивает более быструю кинетику фазового превращения γ→α' при прокатке метастабильной стали AISI 321.

Ключевые слова: аустенитная нержавеющая сталь; водород; двойникование; мартенситное превращение; микроструктура